International Journal of Advances in Scientific Research and Engineering (ijasre)

E-ISSN : 2454-8006

DOI: 10.31695/IJASRE.2022.8.7.3

Volume 8, Issue 7
July - 2022

Machine learning for the prediction and Analysis of Bouguer Gravity anomaly of the Kiri uplift in Congo sedimentary Basin

Raïs Seki Lenzo[1,3], Munezero Ntibahanana[1,2,3], Tondozi Keto[1,3], Moise Luemba[1,2], Gradi Kalonji Lelo[3], Emmanuel Balu Phoba[1,3], Kevin Lumpungu Lutumba[1], Jeaney Lusongo Elua[3,4], Ange Kra[4]

[1]Centre for Research in Géophysique (C.R.G.), Kinshasa, RD Congo

[2]School of Geosciences, China University of Petroleum (East China), Qingdao, 266580, China

[3]Faculty of Oil, Gas and Renewable Energies, University of Kinshasa, DR Congo

[4]National Center for Remote Sensing (CNT), Kinshasa, DR Congo

ABSTRACT

Bouguer gravity anomalies (BGA) play an important role in exploration of mineral resources. Allowing the delineation of large geological structures, BGA participate into discovery of the deposits. However, the Kiri uplift region where several oil seeps have been recognized faces sparse coverage of data due to the difficult conditions of data acquisition on the field. This situation increases the non-uniqueness and nonlinearity problems of the solution using inverse methods. Although, potentially good at quantifying uncertainties, inverse approaches involve enormous computational tasks. We used machine-learning algorithms to predict and analyze gravity data in Kiri uplift region. The algorithms learned to perform as a multiple regression. During training steps, each independent variable included X and Y coordinates, digital elevation model (DEM) and geology. BGA values calculated by experts were provided as the dependent variables. K-fold cross-validation has been used ensure the models are well fit. Since the well-trained algorithms should result in small losses and errors, we experimented several optimizers. By comparison, testing results showed that deep neural network-based algorithm (DNN) has proven to be the most efficient with 5.37 Mean Squared Error and 1.75 Mean Absolute Error as model metrics. DNN showed the most accurate prediction, which, together with the measured BGA reported strongest Pearson correlation coefficient of 0.996. In addition, analysis showed that DNN result is one that conforms perfectly to the regional geology information of the study area. Machine learning algorithms proved their effectiveness to predict and analyze BGA in the study area.

- *ML algorithms proved their effectiveness to predict BGA where measurements lacked*
- *The joint analysis of predicted, measured and regional lithology meets expectations*
- *As predictors are X, Y, DEM and, lithology, we can customize the acquisition grids*

Key Words: *Congo sedimentary basin, Deep learning, Geophysical inversion, Gravity anomalies, Multiple regression.*

1. INTRODUCTION

Gravity prospecting method is sensitive to the anomalous changes of the rock densities into the subsurface [1]. In practice, gravity data are often referred to as (gravity anomalies) which are portions of the measured gravity that deviate from what is expected theoretically. There are many types of gravity anomalies however. In our study, we have been concerned with the so-called Bouguer gravity anomalies [2] that we abbreviate BGA. Indeed, BA have been largely used as an exploration tool for the discovery of petroleum deposits [3, 4]. They have been crucial for analysing deposition areas of the source rocks including hydrocarbon migration paths and locating trap structures of hydrocarbons as well as characterizing the seal rocks above the reservoirs. Overall, realistic maps of BA are involved in the earlier stage of hydrocarbon exploration to select appropriate sites for seismic surveys as well as the placement of the exploration wells. Ultimately, gravity data allow choosing the most economic and efficient options in exploration and development.

This paper studies a case from the Congo basin which undergone several campaigns of oil exploration since 19954's. Results of the previous works, carried out by different experts worldwide revealed the existence of many sedimentation units, oil seeps,

potential source rocks, reservoir rocks and seal rocks [5] in the study area. The Congo sedimentary basin (CSB) is a very large intra-cratonic depression [6,7, 8] covering more than 12,000,000 km^2 [7] in DR Congo. From previous published data, [9] produced a simplified geological map of this basin that shows major sequences of stratigraphic units of the Late Neoproterozoic, Paleozoic and Cenozoic. Having noticed many periods of deformations from existing seismic profiles, [8] came to conclude that the CSB undergone a rifting that was initiated by the subsidence of the Late Proterozoic with a subsequent thermal relaxation. Consequently, this phase resulted in Rodinia breakup, which subdivided the Congo craton along northwest, southeast and northeast, southwest major faults [10]. According to the same authors, two other events of tectonics, which led to the assembly of the Gondwana continent, caused compressional tectonics during the Early Paleozoic Pan-African event [11] and, the Permo-Triassic Gondwanide [8, 12]. However, it might be worth mentioning that gravity data played an important role in the understanding of the regional geology of this basin together with other data. The Kiri uplift and its surrounding areas have been of great interest for petroleum exploration. Mbandaka and Gilson exploration wells in that area reached a massive salt body at 4350 m and 4536 m depths respectively [13]. This massive salt structure may constitute an important target for possible oil traps whose seeps are already highlighted in several sites around that area.

Nonetheless, two main observations motivated our research. On one hand, the acquisition of gravity data in the study area as in the rest of the Congo basin was essentially carried out along rivers and existing roads. Therefore, many areas were not covered by measurements while others were densely covered. This situation cannot allow an effective interpretation of the data. On the other hand, common methods of gravity data interpretation are usually based on the inverse techniques to model the subsurface geology [14, 15]. Unfortunately, when using inverse techniques in geophysics one always faces the non-uniqueness and non-linear problems [16], meaning that, there may exist many models which can fit the measured data equally. Moreover, important variations in the result can be observed when even small variations are made in measured data and, according to [17], a high level of background noise combined with a lack of complete coverage during data acquisition can increases the non-uniqueness of the solution also.

Fortunately, because of their strong ability in non-linear fitting and feature extraction, machine learning (ML) or deep learning (DL) algorithms [18] have proven to be the most powerful method in many fields including object detection, image classification and segmentation [19]. These techniques are still generating a new wave of experiments in many fields including that of geosciences. By using them, many researchers got satisfactory results as illustrated in section 2.2 of this paper. Therefore, in this paper we attempt to train ML algorithms in order to predict and analyze gravity (BGA) around Kiri uplift in accordance to its regional geology. The results of this study will contribute to remotely solve problems of sparse coverage of BGA measurements in the area of study and reduce the weight of the non-uniqueness problem of the solution due to the inverse approach that was used previously as interpretation method. This approach is not reported in the chosen study area yet. In addition, similar works reported in other parts of the world as shown in section 2.2 of this article have been mostly based on classification approaches. In contrast, our chosen algorithms will be trained to perform as multiple regression problems, approach whose, the previous studies did not consider.

2. METHODS AND RELATED WORKS

2.1. Chosen ML Methods

Five artificial intelligence-based algorithms (Ohri, 2017) namely random forest (Brownlee, 2016; Manohar, 2017), decision tree (Manohar, 2017), k-nearest neighbor (Manohar, 2017; Ohri 2017), support vector machine (Rudolph 2018) and deep neural networks (Ohri, 2017; Michie and Spiegelhalter, 1994) have been involved in this study. As the first four algorithms were used as comparison to deep neural network, this section will mainly focus on the last algorithm. It is important to mention that artificial intelligence is a collection of technologies that imitate the way intelligent entities, humans for instance reason and behave in order to implement algorithms that could learn, react and make predictions (Mohaghegh et al., 2018). Currently, those algorithms are used in many fields like medical analysis, financial decision-making, speech and face recognition (Neapolitan and Jiang, 2018) etc. However, some concepts used such, as Machine-Learning (ML) and Deep-Learning (DL) can be confusing. Indeed, the larger concept is artificial intelligence from which ML is derived while DL derived from ML in turn.

DL-based artificial intelligence technology developed rapidly (Pend et al., 2015). Often, it is referred to as "deep neural networks" (DNN) considering the number of layers involved in its architecture. A simple DNN architecture is made of three types of layers: inputs, hidden and output layers. Each layer consists of several artificial neurons. An artificial neuron constitutes the building block of a DNN. It works in the same way as a neuron in the brain of a human. Technically, it can be thought of a simple computational unit, which inputs the weighted predictors, sums them and outputs predictions using an activation function. The activation function serves to govern the threshold at which the neurons are activated and gives the power of the predicted signal. Every weighted predictor has a bias. Often, weights are randomly initialized towards small values. The activation function gives the ability to map the weighted sum to the output neuron.

DOI: 10.31695/IJASRE.2022.8.7.3

In the architecture, all the neurons are linked each to others in a certain fashion (Venkatesan, 2018) where each neuron takes the inputs from the neighboring neurons scaled by their connections in order to be added together and perform some operations. The summed inputs go through an activation function through which, the outputs are passed to the next layer of neurons etc. Traditionally, the nonlinear functions such as logistic or sigmoid are applied as activations allowing the network to combine the inputs in a more complex fashion to provide a rich prediction capability. To summarize, a DNN learns to approximate the function that underlies the relationship between the input predictors and the output predictions, being flexible to match the adopted strategies of the practitioner at the same time. As stipulated by Brownlee (2019) and Manohar (2017), in ML, there exist different types of learning in practice, thus, both supervised and unsupervised regression problems can be handled by traditional ML algorithms as well as DNNs (Goodfellow et al., 2016). This gives to the algorithms an advantage to offer potential applications in geophysics. Problems of which, humans usually perform intuitively can be automatically solved (Neapolitan and Jiang, 2018). In this paper, we have used the supervised regression type of learning. In this approach, we trained the algorithms to cut down a mapping function among inputs and target variables. Every training data point has been labelled with its corresponding target during training. After training, the trained algorithms have been able of making predictions on unseen data (Bishop, 2006). Predictions can be thought as targets retained by the algorithms during their training steps. In other words, the algorithms try to learn patterns that can be used to automatically map input data points to their correct output targets. For doing so, they look for a best hypothesis that will work well on testing data which is data not seen by the algorithm during training but which is part of the training data set. The effectiveness of this best hypothesis is therefore assessed using new data, beyond training and testing data (Russell and Norvig, 2015).

2.2. Related Works

Wang et al. (2019) found that a convolutional neural network can be successfully used to interpolate sparse gravity and magnetic data. Moreover, by using airborne electromagnetic data, Noh et al. (2019) successfully trained a deep neural network to image the subsurface structures. Other authors like Maiti et al. (2020) jointly implemented a Bayesian neural network with variogram modelling using Bouguer anomaly of Eastern Indian Shield in order to reveal the shallow and deeper interfaces in complex geological terrain. Also, in the 80th EAGE Conference and Exhibition of the 2018 year, Dell'Aversana et al. (2018) discussed the possibility of using statistical and classification approaches of machine learning as a supporting workflow, integrating heterogeneous geophysical data that includes seismic, electromagnetic, gravity and well data by combining the approaches of both geophysical modelling and geophysical data inversion. Geophysical Insights carried out a proof of the concept in 2018, evaluating the effectiveness of machine learning in the basin of Denver-Julesburg (Laudon 2019). From the results, it has been found that a multi-attribute machine-learning application improved seismic resolution. A part from gravity and magnetic data, by using the post-stack structural seismic images, convolutional neural networks has been applied to attenuate noise in marine seismic data (Nealon et al., 2019). The output results were much cleaner than the inputs which allowed to highlight geological structures for easier interpretation. Bas et al. (2019) used a multiresolution deep neural network to track seismic horizons. The results showed accurate predictions even in areas located far from the known horizons. A state-of-the-art image processing using machine learning has been applied in 3D seismic fault and salt dome delineation successfully (Wang et al., 2018). According to Zhao and Mukhopanpadhyay (2018) convolutional neural networks are able to capture the structural features of post stack seismic data with good performance than conventional machine-learning. Their workflows for fault detection performed well on challenging synthetic and field data with a high accuracy. By utilising only synthetic seismic images to train the convolutional neural network Wu et al. (2018) accurately estimated fault orientations in seismic images. Salt body delineation is crucial to understand the basin structure and build velocity model for seismic migration. Shi et al. (2019) performed 3-D salt segmentation by using a deep neural network and the results indicated a good capability of capturing subtle salt features from 3D seismic images. Also, Waldeland et al. (2018) discussed how deep learning can be applied for automated seismic interpretation. Likewise, other authors such as Liu et al. (2018) proposed the application of deep-learning litho-facies analysis in seismic data. They found that the approach improves resolution in presence of complex lithology. Even for the interpolation of lithology between wells, geophysical inverse methods based on deep learning have been exploited (Bas et al., 2019). We recall that, this paper is concerned with the application of traditional machine-learning algorithms in comparison with deep neural networks for gravity data prediction and analysis.

3. TRAINING AND TESTING

3.1. Model Fitting

It has been observed that fitting ML or DL model is a challenging task. Generally, the more training data the model is provided with, the better it makes predictions. However, as for supervised learning every training data point is labeled, meaning that outcomes are known, we can compare the predicted results with those labels and change the parameters of the model until both predicted results and labels fit well (Alvishnu, 2017). The main goal here is to give enough ability to the model to successfully generalize and ameliorate its interpretability. The ability to generalize well is crucial. Let us consider that a model has been trained. If this model cannot make accurate predictions on new data, then is useless even if it is able to predict on training data

DOI: 10.31695/IJASRE.2022.8.7.3

accurately. The latter problem is called overfitting (Gupta, 2017). Inversely, the under fitting (Sharma, 2019) happens when the DNN is not provided with enough data in the training step. In this case, the model will even not make predictions accurately on training data. Therefore, the model will not be useful. Therefore, during the training steps, the model needs to be provided with enough data from which it will learn and its parameters have to be set in such way that, the predicted results and labels are close each-others. One of the powerful practices is using cross-validation techniques (Jason, 2020) that we applied to train and test our models.

3.1.1. Data Sets

As shown in Table1, the entire dataset used to train and test the selected models comprises 629 measurements spatially distributed on the study area. These data points are part of the 6000 measurements that were used to produce the first gravity map of the Congo basin, which, helped to get a knowledge on its general structural trends and further, allowed the delineation of several prospective areas for hydrocarbon exploration by the experts of the DR Congo ministry of hydrocarbons. Every input data point is essentially made of a regional geology information whose, distribution is show in Fig.1, a digital elevation model (DEM) as shown in Fig.2 and its corresponding label or target which is the measured value of the Bouguer gravity anomaly (BGA) and whose, the entire distribution is seen in Fig.3.

Table 1. Summary of the data used to train and test the chosen predictive algorithms

	Count	Mean	Std	Min	25%	50%	75%	Max
East long. (meter)	629	881565.7	36098.07	822777	850683	878557	911937	951025
South lat. (meter)	629	9935609	45204.45	9861506	9894856	9933557	9972317	10022148
Lithology	629	1.238474	0.698302	0	1	1	2	2
DEM (meter)	629	330.3355	15.9784	310	318	326	340	385
Gravity (mGal)	629	-32.0894	25.81027	-84.726	-48.646	-32.327	-10.769	19.1059

For the acquisition and processing of the data, Lamont Doherty Geological Observatory, ORSTOM and Kinshasa Meteorological Service were the operators, on behalf of the Congo's government (Kadima et al., 2011). In order to compute the BGAs, measurements were processed using 2.67 gm/cm^3 of reduction.

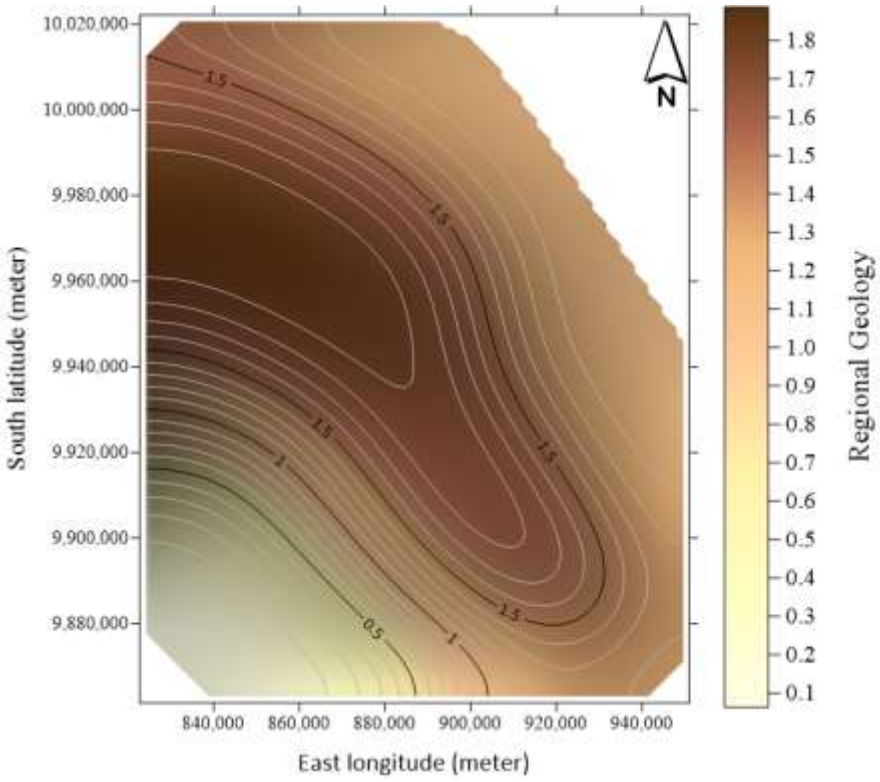

Figure 1. Map of the spatial variation of the regional geology in the study area. As seen on the color bar, geology varies from zero to two. For all the three types of lithology in the study area, the Quaternary is given the value of zero, one for the Tertiary and 2 for the Cretaceous.

DOI: 10.31695/IJASRE.2022.8.7.3

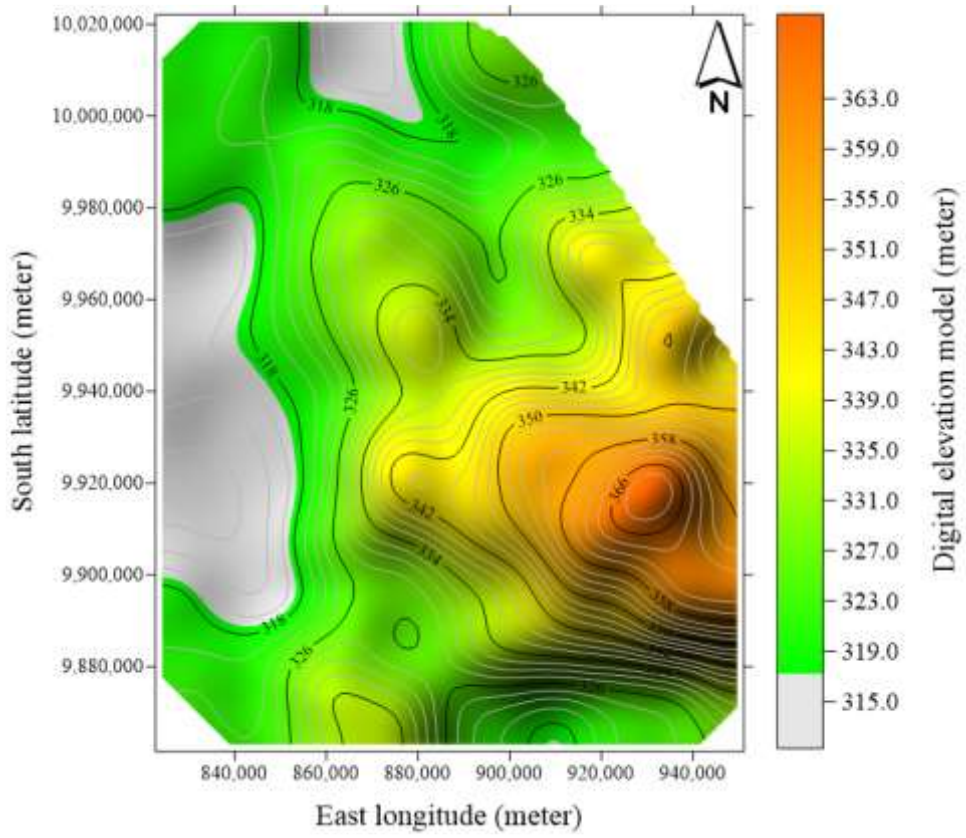

Fig. 2. Map of the spatial variation of the digital elevation model (DEM). Almost, three distinct regions are seen on the map. High values are mostly localised in the southwest of the study area and lowest values mostly in the west part. Distribution is showing to be correlating with the regional geology.

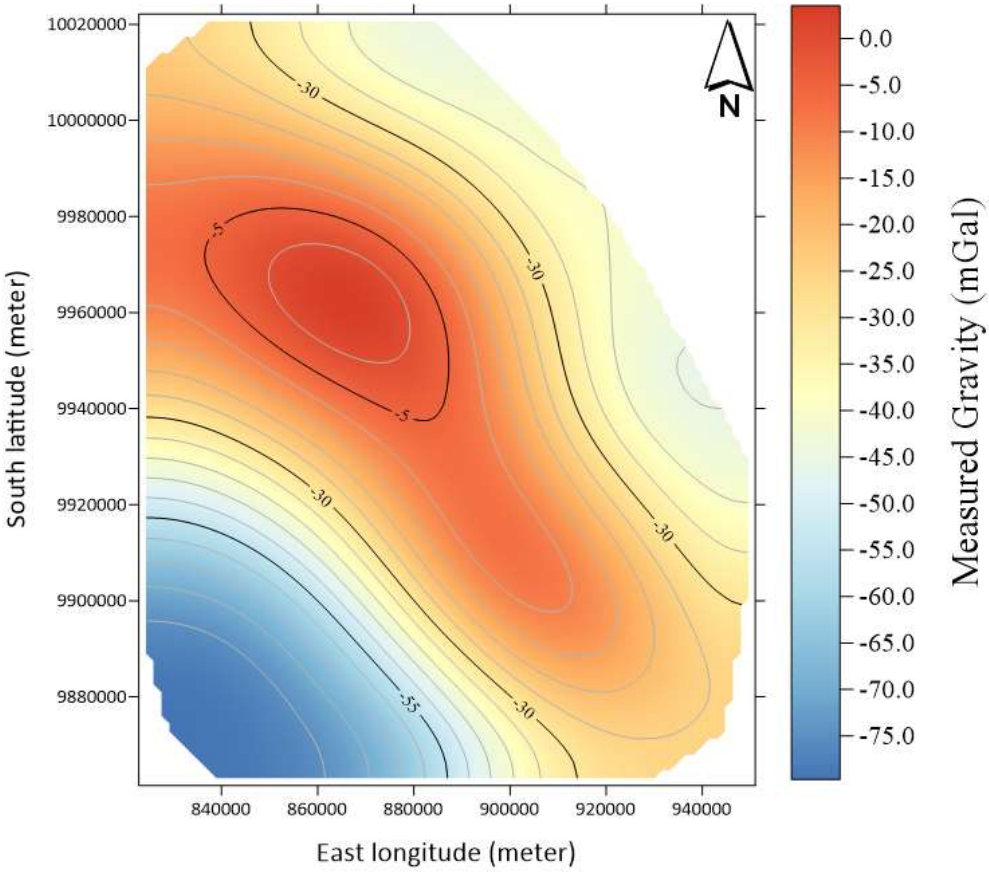

Fig. 3. Map of the spatial distribution of the BGA. As for geology and DEM, almost, three distinct regions are seen on the map. In contrast with the DEM distribution, high gravity values are mostly located in the northern-west of the study area and lowest values mostly in the southern-west. The distribution shows well correlation with the regional geology.

DOI: 10.31695/IJASRE.2022.8.7.3

In order to ensure good fitting of the chosen models, we applied the k-fold cross-validation technique to get where the number of folds was defined to be five. Randomly, Table 2 shows an example of a set reserved for training purpose only.

Table 2. Summary of the data set used to train the chosen algorithms, randomly chosen.

	Count	Mean	Std	Min	25%	50%	75%	Max
East long. (meter)	503	882102.3	36132.58	822777	850690	878558	911946	951025
South lat. (meter)	503	9934328	45317.04	9861506	9894818	9933523	9972310	10022148
Lithology	503	1.232604	0.711019	0	1	1	2	2
DEM (meter)	503	330.6402	16.3084	310	318	326	340	385

However, the relationship between the labels namely made of digital elevation model, latitude and gravity with geology is show in Fig.4. In addition, the summary of the testing data set, randomly chosen is shown in Table 3.

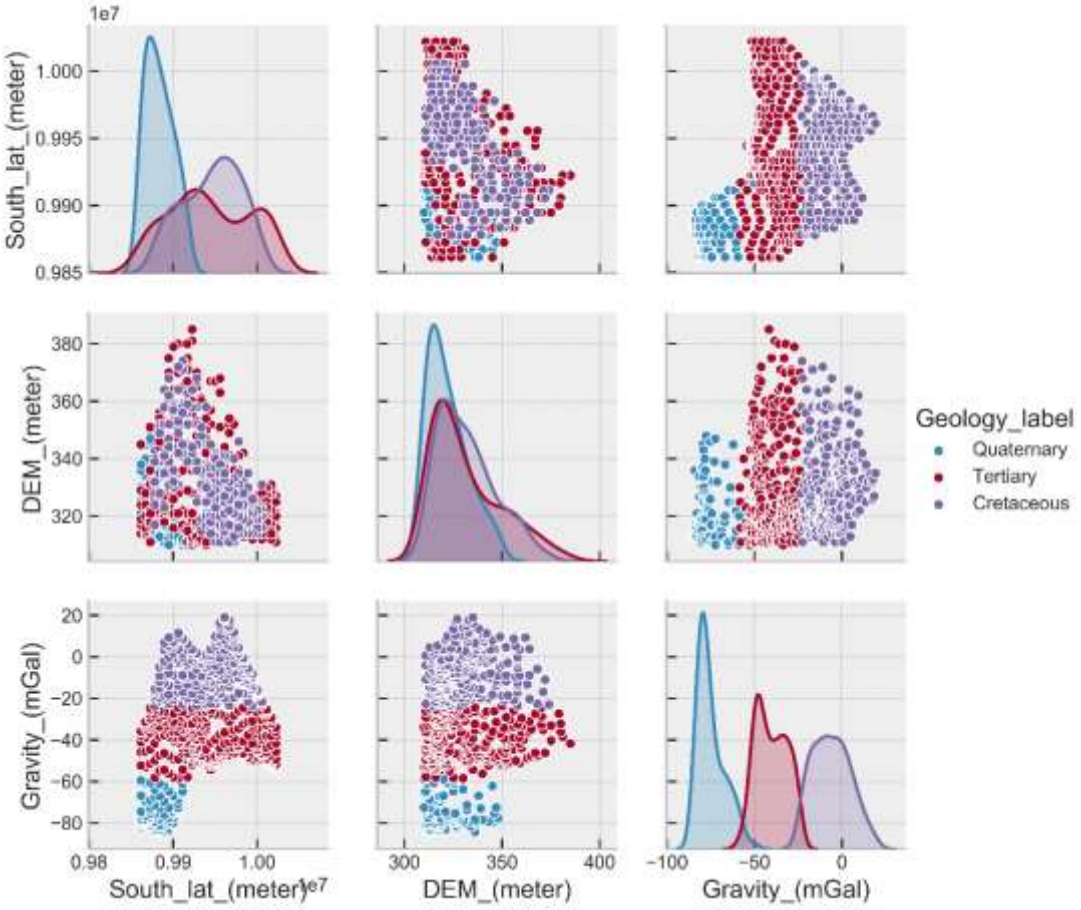

Fig. 4. A pair plot of the training data set. We can see the relationship between DEM, gravity and latitude in accordance with the regional geology: gravity is weakly increasing with the increase of the DEM while is still high in cretaceous and low in quaternary. In addition, the decrease in latitude implies an increase in gravity.

Table 3. Summary of the data set used to test the trained algorithms, randomly chosen.

	count	mean	Std	min	25%	50%	75%	max
East long. (meter)	126	879423.4	36023.61	822792	846500.3	878498	910544.5	951013
South lat. (meter)	126	9940722	44563.44	9861523	9900384	9939115	9977850	10022146
Lithology	126	1.261905	0.647192	0	1	1	2	2
DEM (meter)	126	329.119	14.58416	310	317.25	326	337	379

3.1.2 Optimizer and Loss

The supervised DNN training is an optimization problem. This process aims to find the lowest loss and error that express how efficient the trained DNN is. To minimize losses and errors and, to prevent the overfitting phenomena, we have experimented with different optimization functions namely the Stochastic Gradient Descent or SGD (Bottou and Bousquet, 2012), the Root Mean

DOI: 10.31695/IJASRE.2022.8.7.3

Squared Propagation also called RMSProp (Geoffrey 2020), the Adam or Adaptive Moment Estimation (Heusel et al., 2017) and the Nadam or Nesterov Accelerated Adaptive Moment Estimation (Dozat, 2016). It is good to mention that, the well-chosen optimization and loss functions allow the DNN to make optimum and faster prediction. Optimizers update weights and biases of the DNN to reduce its error. In addition, we have defined the Mean Squared Error (MSE) (Mishra, 2018) in Eq. (1) to be the loss function. The latter expresses the squared average of the difference between labels and predicted results. In this equation y_j represents the labels and $\hat{y}_j$, the predicted results.

$$MSE = \frac{1}{N}\sum_{j=1}^{N}\left(y_j - \hat{y}_j\right)^2 \quad (1)$$

Finally, the Nadam optimization function resulted in the best results as shown in Fig.5. The trained DNN model achieved very small errors on both the training and testing sets while it is still prevented from the overfitting. When the testing value of loss is lesser than that of training one, we say that the model is overfitting.

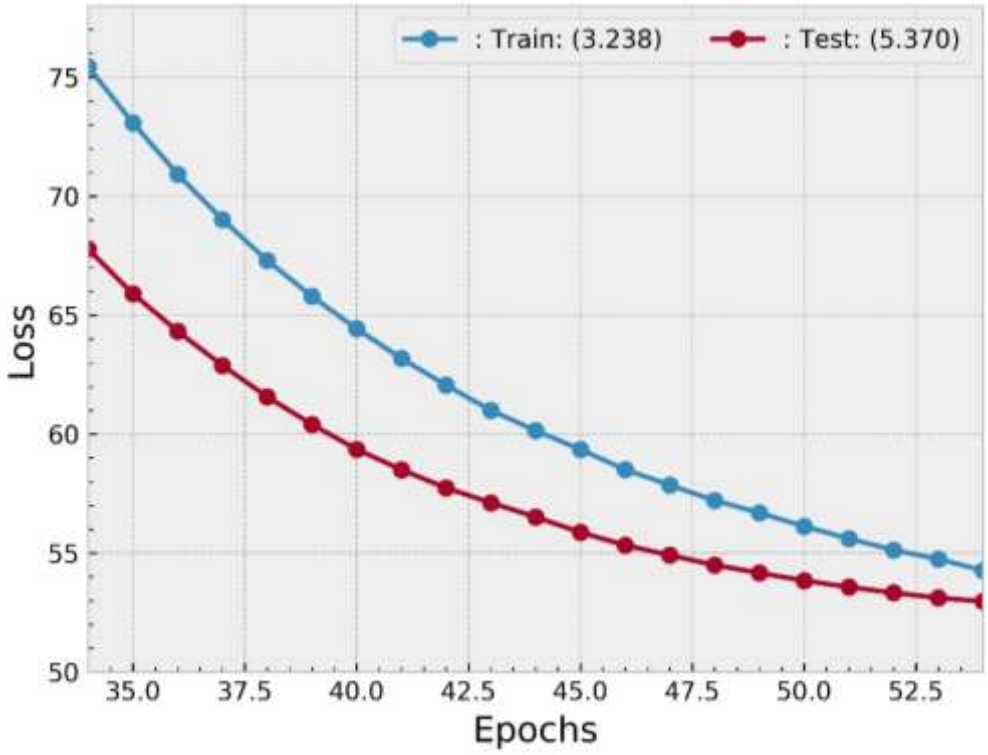

Fig. 5. The Mean Squared Error-loss of the trained DNN model with different optimization functions. The training and testing losses are decreasing with the number of epochs. Nadam optimizer resulted in smallest loss and kept the small gap between training and testing loss values. The algorithm was trained on 3000 epochs thus for visualization purpose we displayed the scenario between 35 and 53 epochs.

3.2. Metric Functions

The well-trained algorithms should result in small errors. Indeed, in the real life we are always interested on how well the models will perform on new data. This determines the real-world performance of the algorithms. In other words, a model that performs well on data that it has not seen before, generalizes well and its error is small as well. That is the reason why, all the performance metrics have to be calculated on the testing data that are separated from those used in real training step.

However, Bouguer anomalies are continuous variables. Since then, we can use the Mean Absolute Error (MAE) to assess the performance of the trained models. MAE is measure of the error between a pair of observations which express the same phenomenon. This metric has the advantage of not considering the directions of those variables. The MAE as expressed in Eq. (2) is therefore an arithmetic average of the absolute error values between the predicted results $\hat{y}_i$ and the corresponding labels y_i. It is a linear score in which all the individual differences are equally weighted in the average.

$$MAE = \frac{\sum_{i=1}^{n}|\hat{y}_i - y_i|}{n} = \frac{\sum_{i=1}^{n}|e_i|}{n} \quad (2)$$

DOI: 10.31695/IJASRE.2022.8.7.3

Among all the optimizers that we experimented, Nadam optimiser have resulted in smallest MAE for the DNN as shown in Fig.6 and prevented models from overfitting. When the testing error value is lesser than that of training one, we say that the model is overfitting.

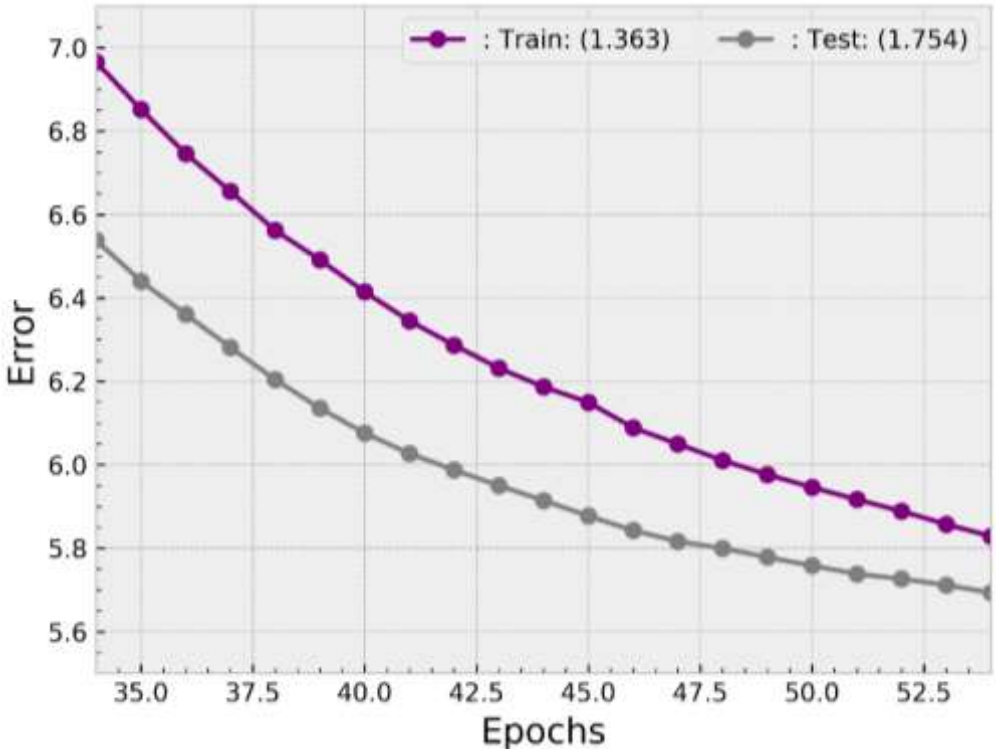

Fig. 6. The Mean Absolute Error of the trained DNN model with different optimization functions. The training and testing errors are decreasing with the number of epochs. Nadam optimizer resulted in smallest loss and kept the small gap between training and testing loss values. The algorithm was trained on 3000 epochs thus for visualization purpose we displayed the scenario between 35 and 53 epochs.

Another metric that we used is the Root Mean Squared Error (RMSE) defined in Eq. (3) and which is a quadratic scoring rule that uses to square the errors before they can be averaged. In comparison with the MAE, the RMSE gives high weight to large errors, for this reason it is useful where large errors are undesirable. In the equation y_i and x_i are predicted and measured gravity respectively.

$$RMSE = \sqrt{\frac{1}{n}\sum_{i=1}^{n}(y_i - x_i)^2} \qquad (3)$$

For the RMSE metric, the same Nadam optimizer has been good to minimize errors and prevent the models from overfitting.

As said previously, a K-fold cross-validation technique whose metric results are shown in Table 4 has been applied to split original data into real training and testing sets that have been used to train traditional ML models. This can be taken as a procedure for resampling the data and, it is useful to assess machine-learning models where there are limited data samples. The parameter k is referring to how many groups into which our original data is going to be split. Therefore, when a given value for k is defined, it may be used to replace k in the reference to the algorithm, such as k equals 5 that becomes 5-fold cross-validation. It is a very popular technical since it usually results in a less biased estimation of the skill of the model than any other technique, such as the train/test split technique.

Table 4. The k-folds cross-validation metric results for the chosen traditional machine learning algorithms.

Models	Cross-validation	Datasets	Evaluation metrics

DOI: 10.31695/IJASRE.2022.8.7.3

	K-fold	Training set	Testing set	MAE	MSE	RMSE	Mean MAE
Random Forest	1	503	126	-3.25	-20.3	-4.51	1.75
	2	503	126	-2.88	-16.4	-4.05	
	3	503	126	-2.82	-15.6	-3.96	
	4	503	126	-2.96	-18.5	-4.31	
	5	504	125	-3.30	-19.9	-4.46	
	K-fold	Training set	Testing set	MAE	MSE	RMSE	Mean MAE
Support Vector Machine	1	503	126	-21.4	-687	-26.2	4.62
	2	503	126	-22.4	-739	-27.1	
	3	503	126	-21.2	-667	-25.8	
	4	503	126	-19.0	-524	-22.8	
	5	504	125	-22.6	-713	-26.7	
	K-fold	Training set	Testing set	MAE	MSE	RMSE	Mean MAE
K Neighbors	1	503	126	-1.63	-4.55	-2.13	1.27
	2	503	126	-1.90	-6.46	-2.54	
	3	503	126	-1.49	-4.02	-2.00	
	4	503	126	-1.62	-4.68	-2.16	
	5	504	125	-1.45	-3.77	-1.94	
	K-fold	Training set	Testing set	MAE	MSE	RMSE	Mean MAE
Decision Tree	1	503	126	-4.69	-47.0	-6.85	2.05
	2	503	126	-4.38	-33.8	-5.82	
	3	503	126	-3.77	-26.6	-5.15	
	4	503	126	-4.23	-33.8	-5.82	
	5	504	125	-3.98	-25.7	-5.07	

4. RESULTS AND DISCUSSIONS

4.1. Results

The testing results from all the trained algorithms are reported here. The analysis is done in this section too. We used different kind of visualizations for the purpose. In first, we have computed a pairplot as seen in Fig.7, which visualizes pairwise the results to find the relationships between predictions and measured or true gravity of the study area. A pairplot is a module integrated of seaborn library in python that gives a high-level interface to draw informative and attractive statistical results (Sarath, 2019). In fact, from this pairplot, variations can be observed through each sub-plot. Note that, sub-plots are in matrix format in which the x axis is represented by the row name and the y axis by column name. The diagonal of this plot shows sub-plots, which are distributions of the univariate kernel density of the features.

DOI: 10.31695/IJASRE.2022.8.7.3

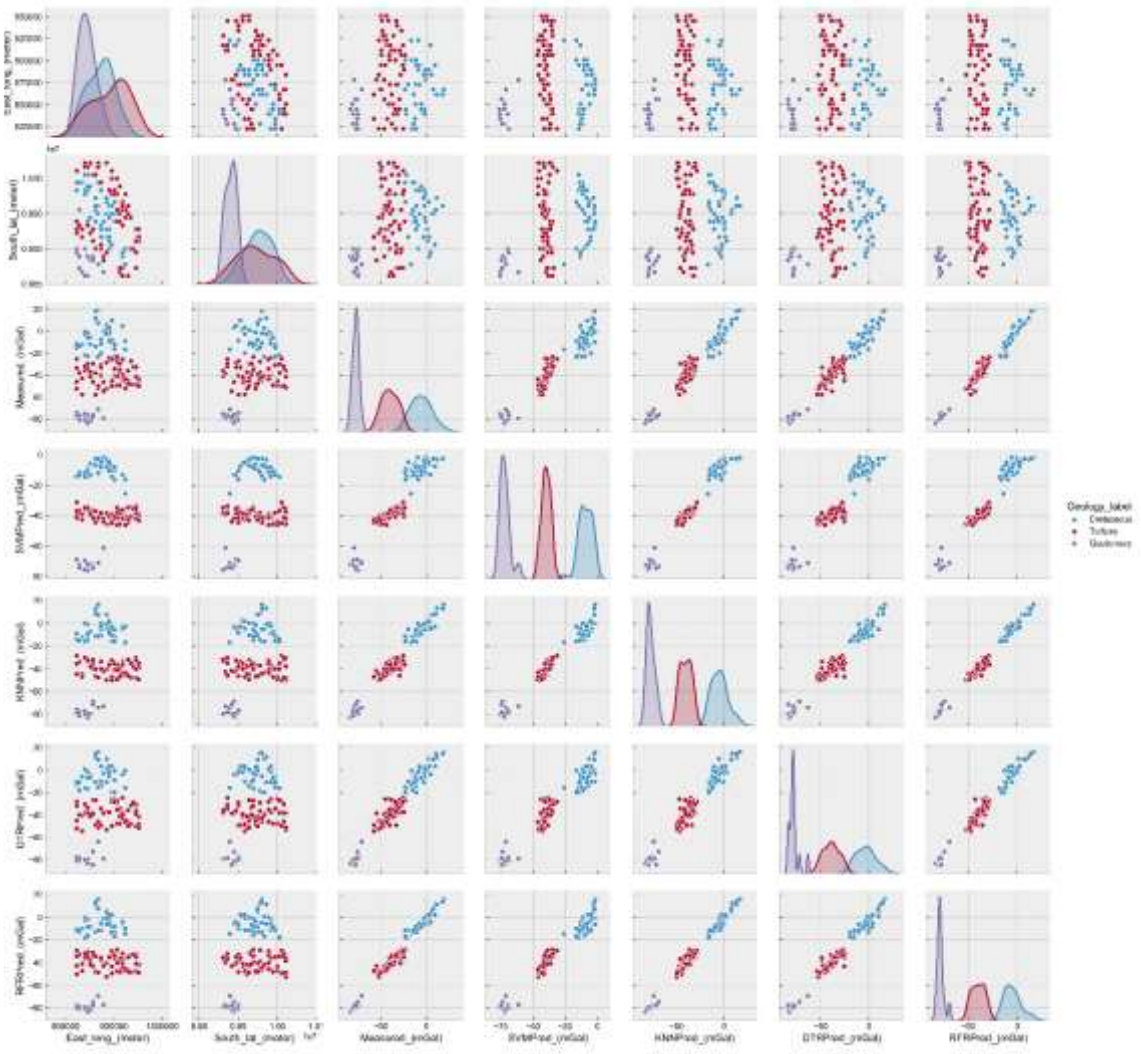

Fig. 7. Compared to measured gravity, all the models showed good result. Random forest has the best performance followed by k-nearest neighbor while Decision tree results are less accurate than those of the two previous models are. In turn, Support vector machine result is not good as that of Decision tree. All the results correlate the regional geology of the study area.

In addition to the pairplot, we computed Pearson correlation coefficients, which are reported in Table 5. This is a way of quantifying the relationship between the predicted results and, the measured or true gravity of the study area. These coefficients take values between -1 that indicates a negative linear correlation which is perfect and 1 that indicates a positive linear correlation which is also perfect. When the coefficient is zero, there is no linear correlation (Zach, 2020). The closer the coefficients are to one, the stronger the relationship between the predicted result and the measured gravity.

Table 5. Pearson correlation coefficients between the predicted results of the trained traditional machine learning algorithms and the measured gravity of the study area

	Measured	SVM Pred.	KNN Pred.	DTR Pred.	RFR Pred.
Measured	1.00	0.96	0.98	0.975	0.99
SVM Pred.	0.96	1.00	0.98	0.962	0.98
KNN Pred.	0.98	0.98	1.00	0.974	0.99
DTR Pred.	0.98	0.96	0.97	1.000	0.99
RFR Pred.	0.99	0.98	0.99	0.986	1.00

From the above table we observed that random forest predictions (RFR Pred.) has the strongest correlation with the measured gravity followed by k-nearest neighbor predictions (KNN Pred.), decision tree predictions (DTR Pred.) and support vector machine predictions (SVM Pred.) at last position. However, based on values of those coefficients, all the predictions have strong correlation with the mesured gravity. In order to give more clear idea of how these predictions are spatially distributed in accordance to the measured gravity, we have drawn the following gravity maps: random forest prediction map in Fig.8, support

DOI: 10.31695/IJASRE.2022.8.7.3

vector machine prediction map in Fig.10, k-nearest neighbor prediction map in Fig.12 and decision tree prediction map in Fig.14. These maps highlight small differences with the map of the measured gravity.

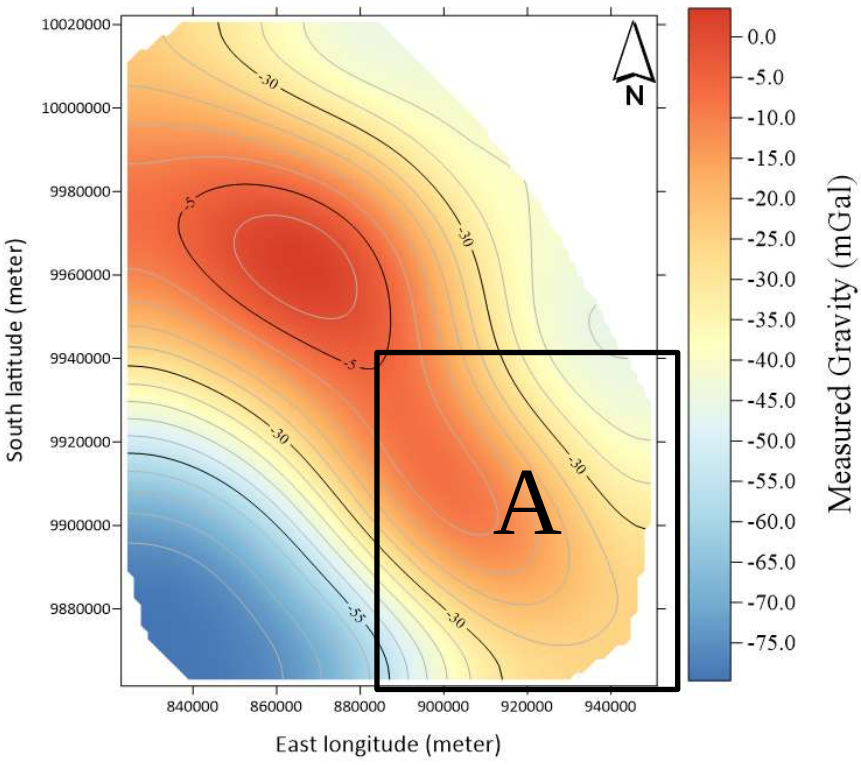

(b) Measured gravity

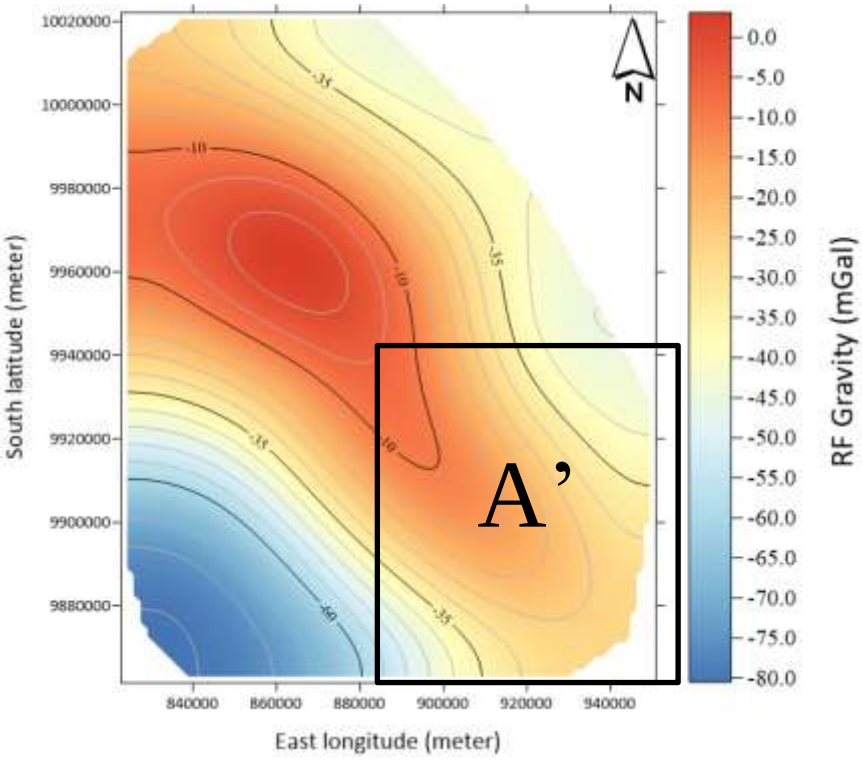

(b) Random forest algorithm prediction

Fig. 8. The spatial distribution map of the random forest result. Measured gravity map (a) show almost the same distribution as that of random forest prediction map (b). Measured gravity ranges from -75 mGal to zero mGal while random forest gravity ranges from -80 mGal to zero mGal and gravity field weakens towards southeast. For instance, compare A, and A' on the maps.

Let us recall that all the algorithms have been trained on top of regional geology of the study area. To know in which geology the random forest model predict well we computed the lmplot in Fig.9, which is, intended to be intensively convenient in regression

DOI: 10.31695/IJASRE.2022.8.7.3

model fitting across subsets of the whole dataset. The lmplots for support vector machine, k-nearest neighbor and decision tree models are shown in Figs.11, 13 and 15 respectively.

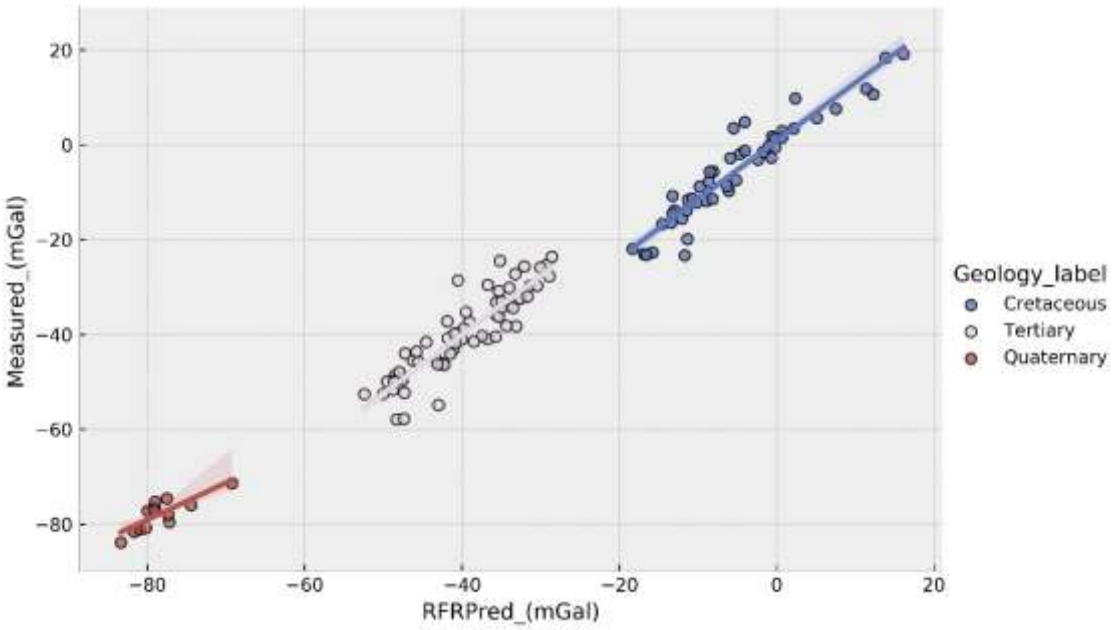

Fig. 9. The lmplot of the random forest prediction and the measured gravity in relationship with regional geology. Good linear fitting of the random forest prediction to the measured gravity can be observed across geology thus, the best fitting is in tertiary, followed by cretaceous and finally, the quaternary.

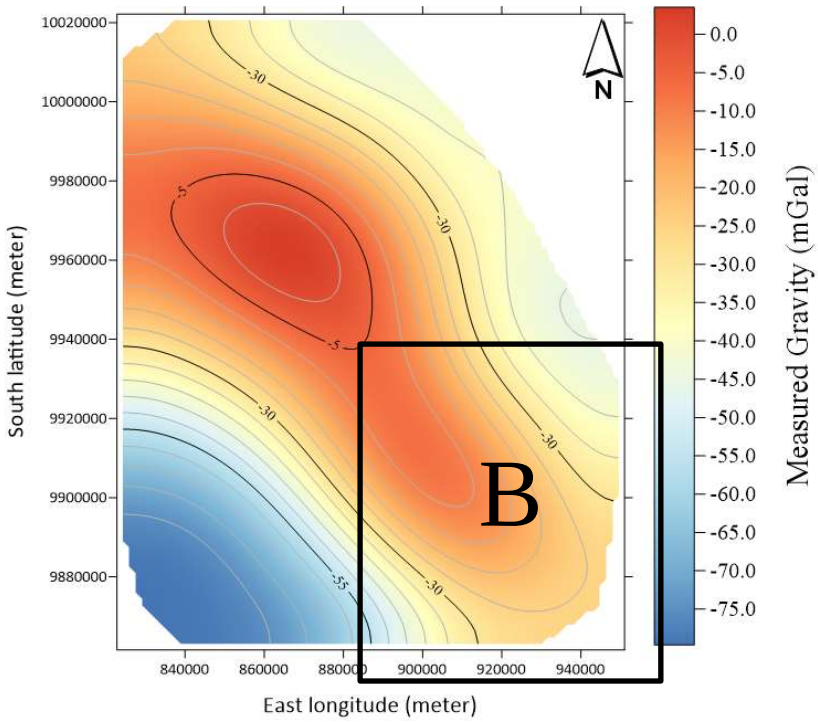

(b) Measured gravity

DOI: 10.31695/IJASRE.2022.8.7.3

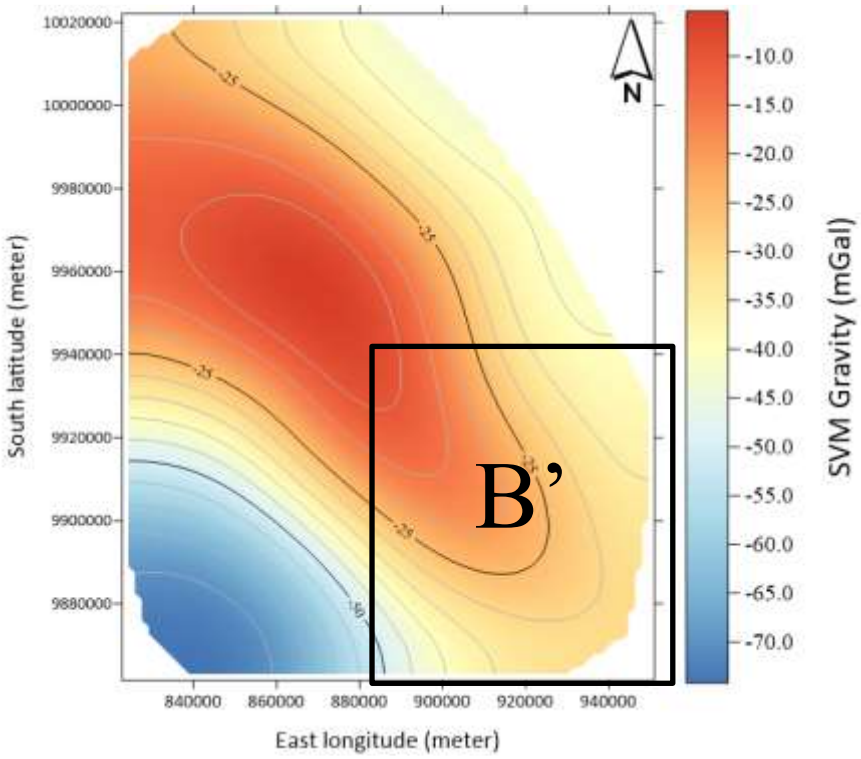

(b) Prediction of the support vector machine

Fig. 10. The spatial distribution map of result the support vector machine. Measured gravity map (a) show differences in the distribution in relation to that of support vector machine prediction map (b). Measured gravity ranges from -75 mGal to zero mGal while support vector machine gravity ranges from -70 mGal to -10 mGal. Gravity field weakens towards southeast and northeast. For instance, compare B and B' on the maps.

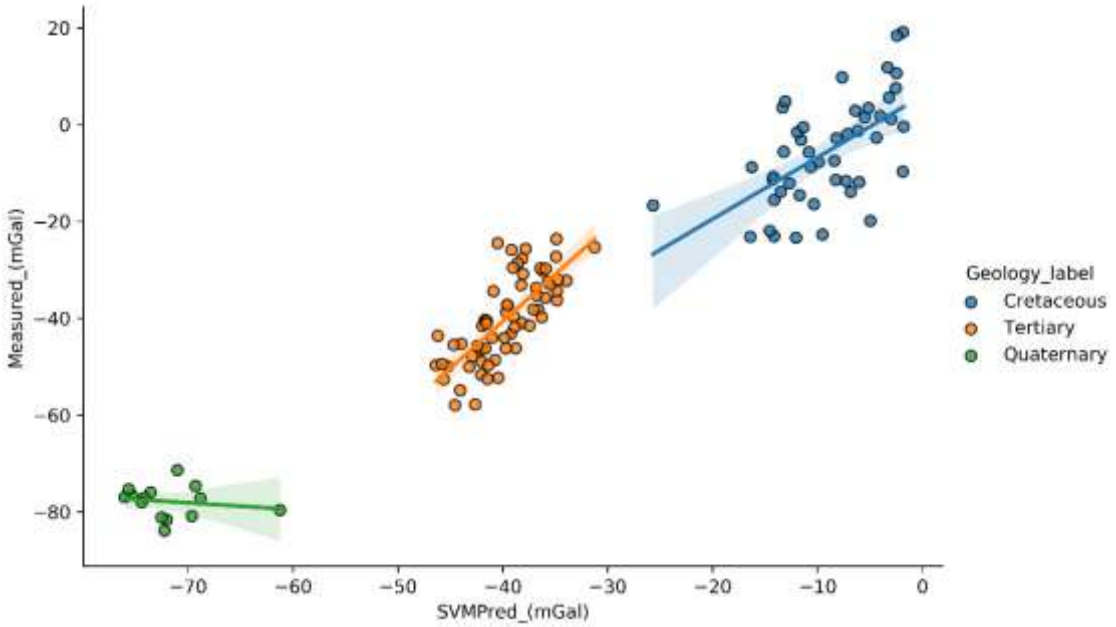

Fig. 11. The lmplot of prediction of the support vector machine and the measured gravity in relationship with regional geology. Good linear fitting of the prediction to the measured gravity can be observed in tertiary only.

DOI: 10.31695/IJASRE.2022.8.7.3

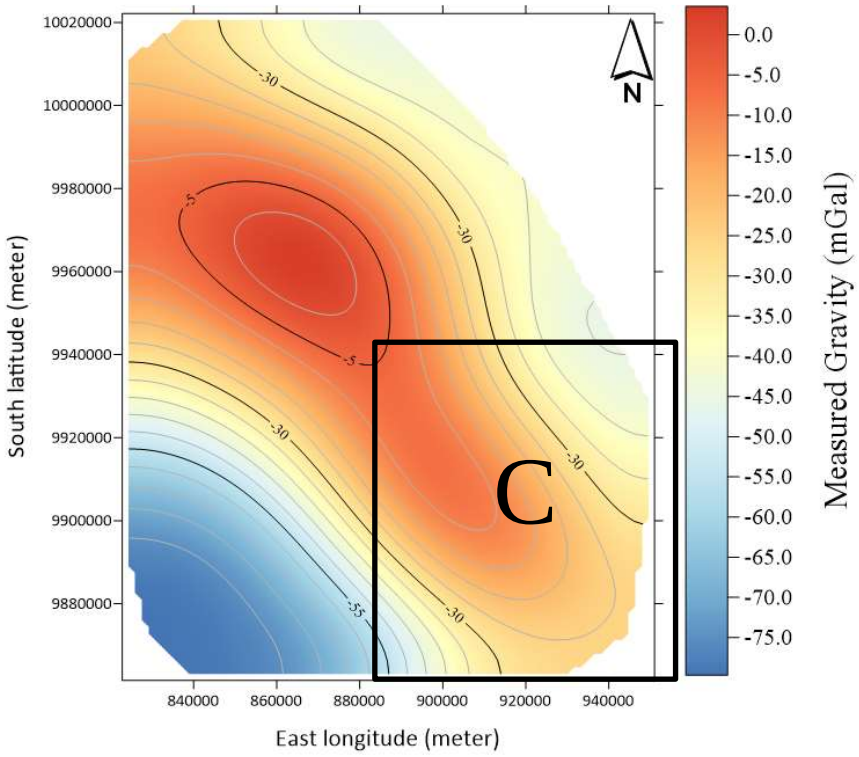

(a) Measured gravity

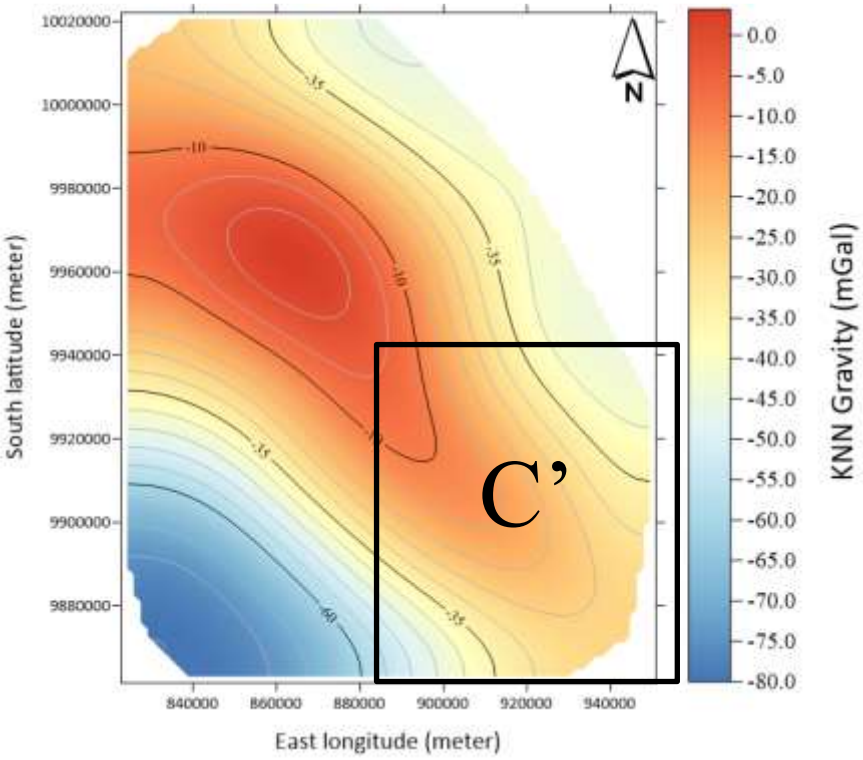

(b) k-nearest neighbor algorithm prediction

Fig. 12. The spatial distribution map of the k-nearest neighbor result. As for random forest result, measured gravity map (a) shows almost the same distribution with to that of the k-nearest neighbor prediction map (b). Measured gravity is still ranging from -75 mGal to zero mGal and k-nearest neighbor gravity from -80 mGal to zero mGal too. The same, gravity field weakens towards southeast. For instance, compare C and C' on the maps.

DOI: 10.31695/IJASRE.2022.8.7.3

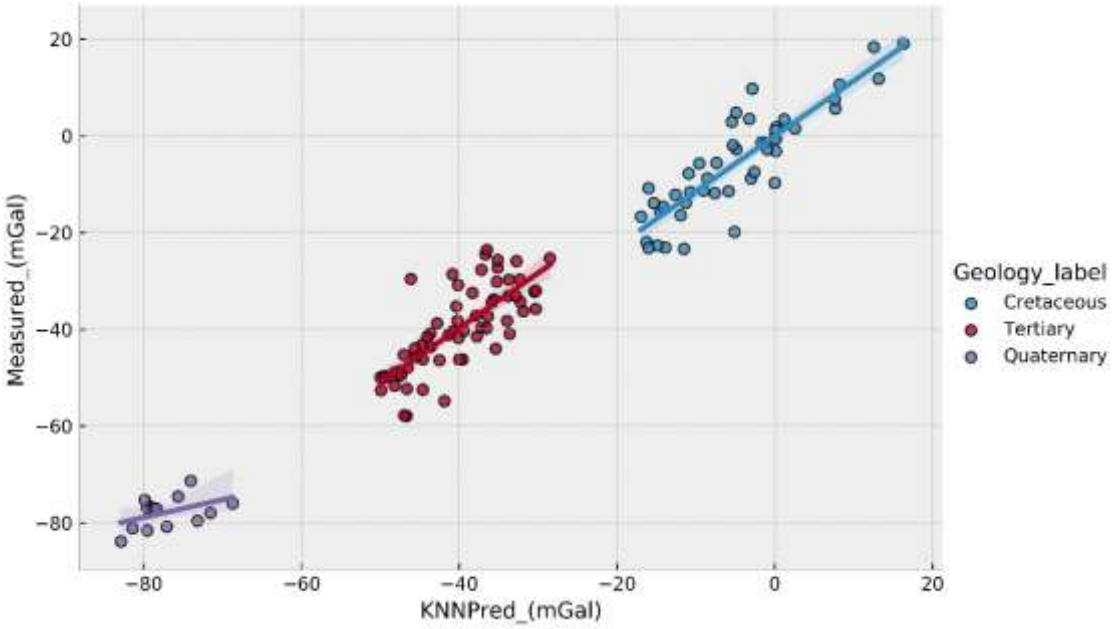

Fig. 13. The lmplot of the k-nearest neighbor result and the measured gravity in relationship with regional geology. Good linear fitting of the k-nearest neighbor prediction to the measured gravity can be observed across geology thus, the best fitting is still in the tertiary as for random forest, followed by the quaternary instead of cretaceous.

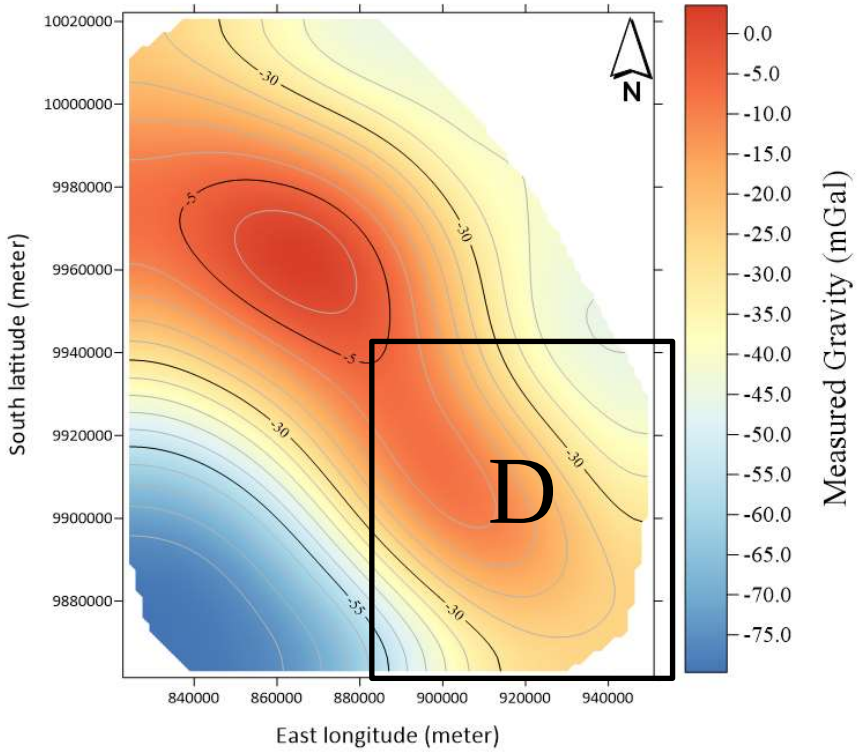

(a) Measured gravity

DOI: 10.31695/IJASRE.2022.8.7.3

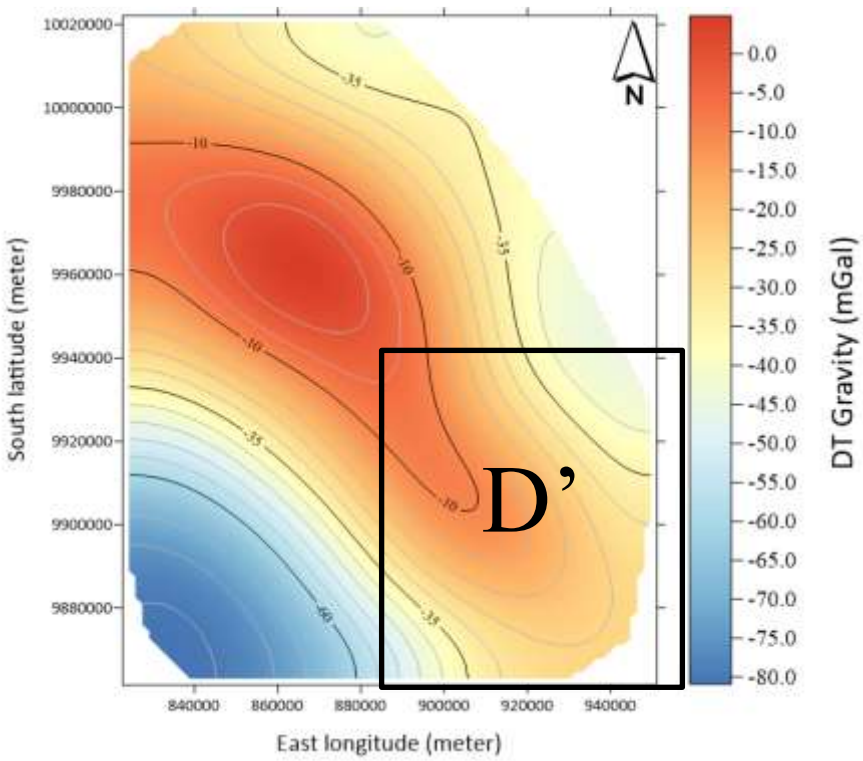

(b) Decision tree algorithm prediction

Fig. 14. The spatial distribution map of the decision tree result. Apart from random forest, k-nearest neighbor and support vector machine results, measured gravity map (a) shows obvious differences in relation to that of the decision tree prediction map (b). Measured gravity is still ranging from -75 mGal to zero mGal and decision tree gravity from -80 mGal to zero mGal as for k-nearest neighbor and random forest thus, gravity field weakens towards southeast and northeast. For instance, compare D and D' on the maps.

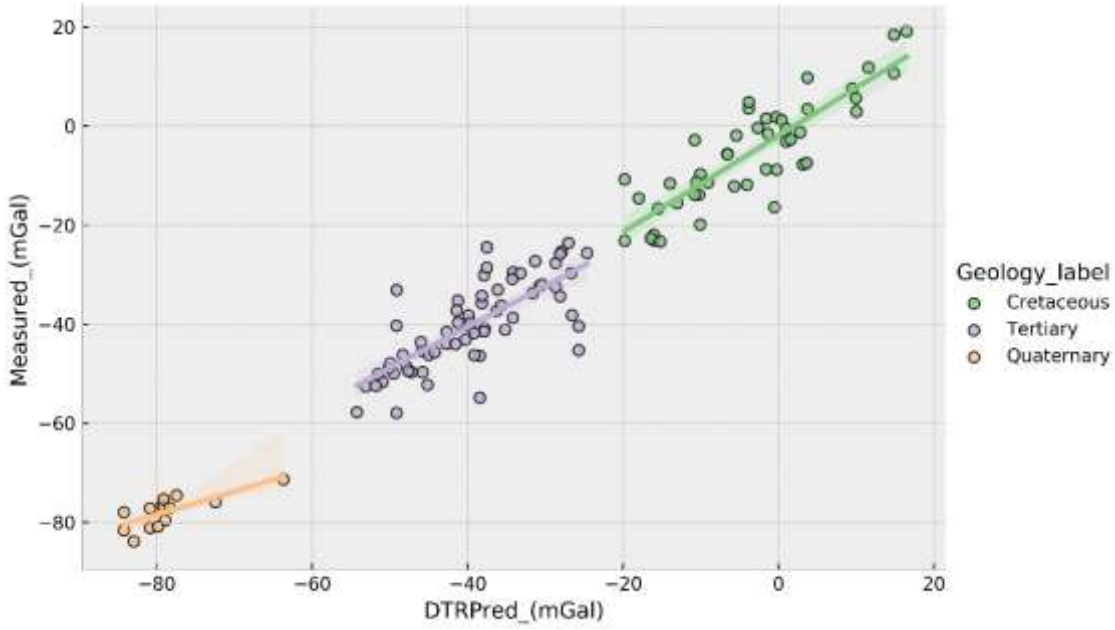

Fig. 15. The lmplot of the decision tree result and the measured gravity in relationship with regional geology. Relative good linear fitting of the decision tree prediction to the measured gravity can be observed across geology. In contrast to the other models, prediction fits almost equally in all types of geology but this model seems to perform well in quaternary.

4.2. Discussions

DOI: 10.31695/IJASRE.2022.8.7.3

We could not find ML-based works reported in the study area previously so that we may compare our result to those. Apart from what is listed in section 2.2, Using ML or DL algorithms many other research works (Otchere et al., 2020) have been conducted to either classify facies or predict some properties of hydrocarbon reservoir and showed good results. A same approach to what we achieved in this paper could be that of Dell'Aversana (2019) who used five supervised ML algorithms to comparatively classify lithofacies based on multiple logs from two wells and found that his methodology is particularly useful to quickly predict or classify lithofacies when it is required in real-time decision-making. Likewise, our trained algorithms give consistent results in milliseconds and can work on simple computers, allowing making interpretation in short time. The other published works to comparing the machine learning tools report the classification of rock facies using the gradient boosting algorithm (Zhang and Zhan, 2017) which was effective on two test well data. Before we conclude the study, our traditional ML-based results have been compared to the result of deep neural network DNN that is recognized to be the most powerful tool in the field of ML. For the purpose, an analysis of the Pearson correlation coefficients (Table 6) is done and lmplot of the DNN result (Fig.17) against measured gravity have been computed. Spatial distribution of the latter is shown in Fig.16 too. Although, random forest showed strongest positive correlation to measured gravity among traditional ML algorithms but DNN result is shown to be the best of all the trained algorithms.

Table 6. Pearson correlation coefficients between the predicted results of the trained traditional ML algorithms, DNN result and the measured gravity of the study area.

	Measured	MRNN Pred.	SVM Pred.	KNN Pred.	DTR Pred.	RFR Pred.
Measured	1.000	0.996	0.956	0.976	0.975	0.987
MRNN Pred.	0.996	1.000	0.963	0.980	0.977	0.991
SVM Pred.	0.956	0.963	1.000	0.982	0.962	0.979
KNN Pred.	0.976	0.980	0.982	1.000	0.974	0.992
DTR Pred.	0.975	0.977	0.962	0.974	1.000	0.986
RFR Pred.	0.987	0.991	0.979	0.992	0.986	1.000

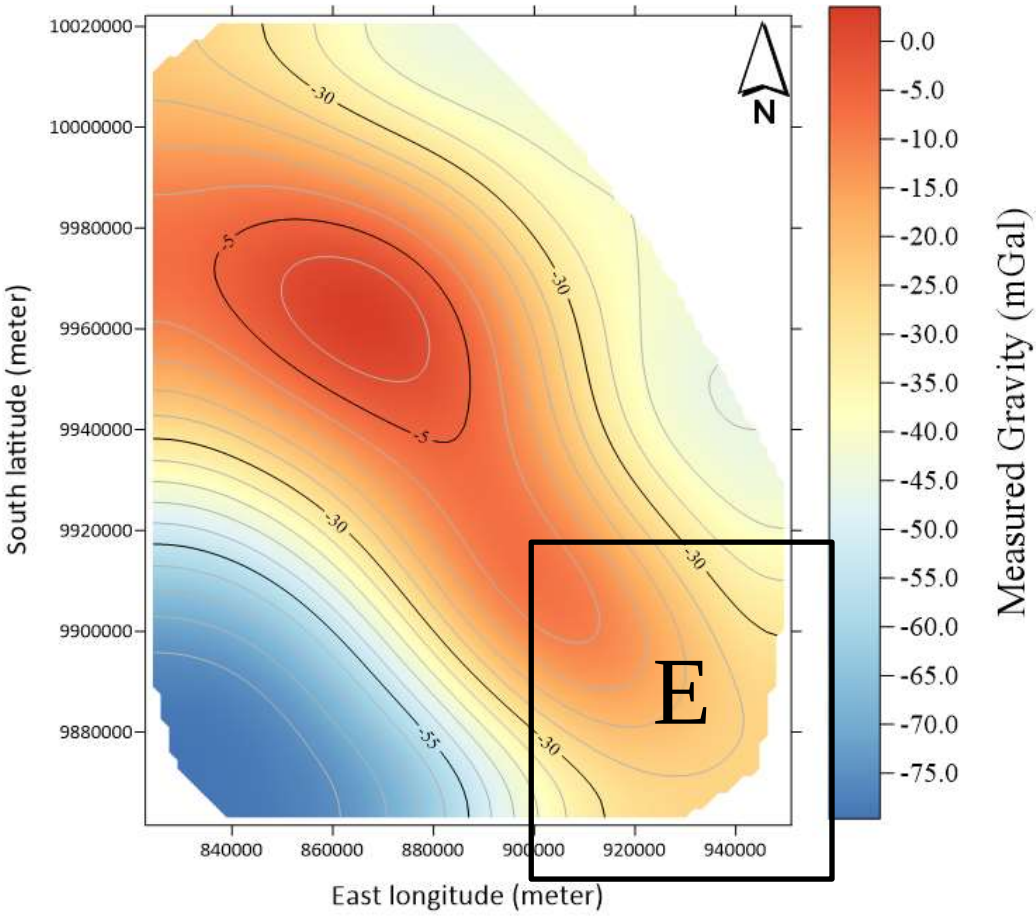

(a) Measured gravity

DOI: 10.31695/IJASRE.2022.8.7.3

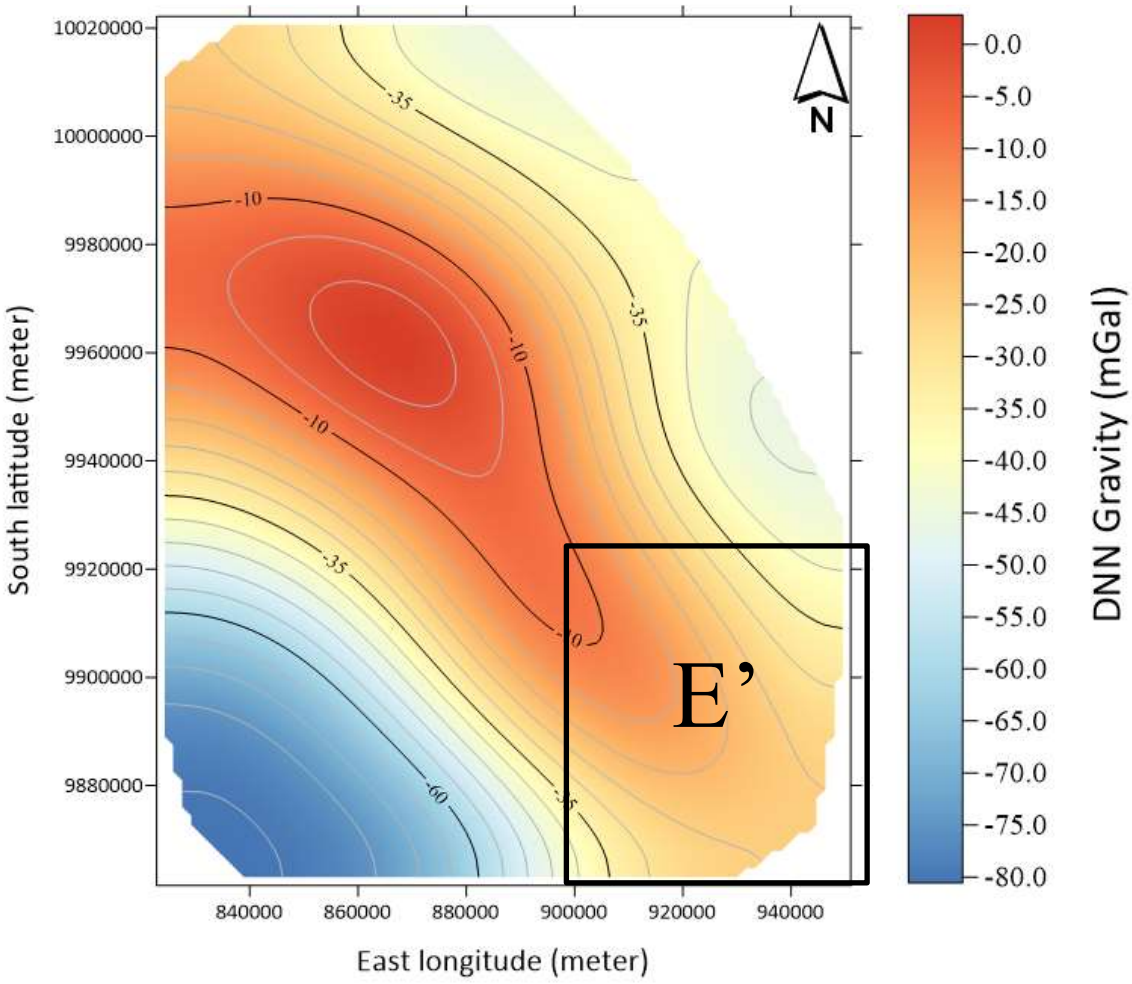

(b) Decision tree algorithm prediction

Fig. 16. The spatial distribution map of the deep neural network result. The measured gravity map (a) does not show any difference with that of the deep neural network prediction map (b). Measured gravity is still ranging from -75 mGal to zero mGal and deep neural network gravity from -80 mGal to zero mGal as for k-nearest neighbor and random forest thus, gravity field does not weaken towards southeast nor northeast as in previous cases. For instance, compare E and E' on the maps.

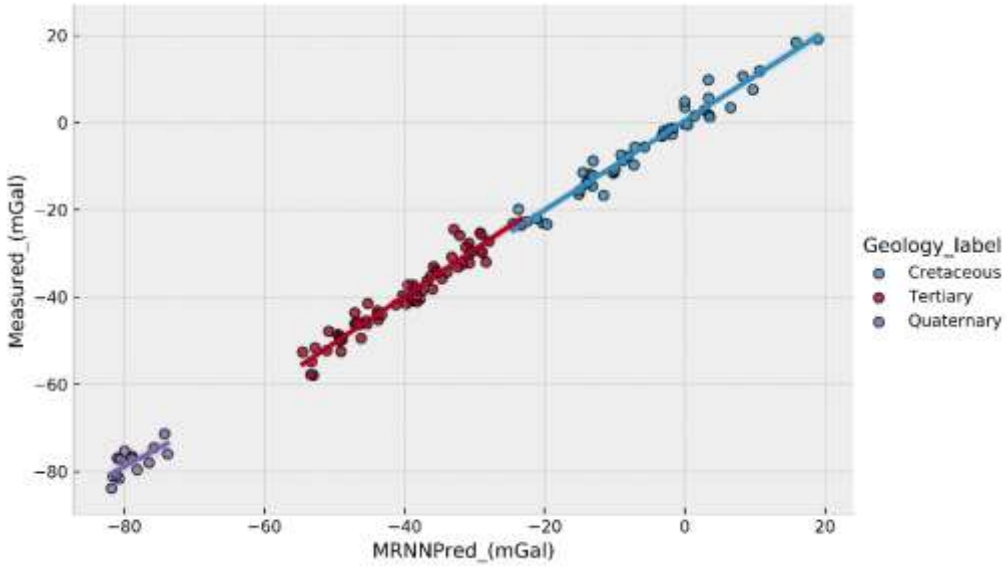

Fig. 17. The lmplot of the deep neural network and the measured gravity in relationship with regional geology. Good linear fitting of the deep neural network prediction to the measured gravity can be observed across all types of geology. In contrast to the other models, prediction fits equally in all types of geology.

DOI: 10.31695/IJASRE.2022.8.7.3

5. CONCLUSIONS

Using geographic coordinates, digital elevation model and regional geology information, we have trained five supervised machine learning algorithms to efficiently predict and analyze gravity in Kiri uplift region of the Congo basin. Although all the chosen algorithms resulted in some small differences regarding their evaluation metrics thus, the testing results showed that they are all efficient enough to predict gravity. Approximatively, all the testing results correlated well the regional geology of the study area. For the traditional ML algorithms, RF showed the best result. Its prediction showed a Pearson correlation coefficient of 0.99, followed by k-NN with 0.98. DT and SVM had less performance than those of the two previous algorithms with Pearson correlation coefficients of 0.97 and 0.96 respectively. The spatial distribution maps of the predicted results showed almost the same distribution as that of the measured gravity thus, small differences have been observed towards southeast on random forest and k-NN prediction maps where gravity values ranged from -80 mGal to zero mGal towards southeast while measured gravity value ranged from -75 mGal to zero mGal. Important differences have been noticed on the spatial distribution map of SMV. The predicted gravity values ranged from -70 mGal to -10 mGal towards southeast and northeast. Those of DT showed the same trend while ranging between -80 mGal and 0 mGal as for k-NN and RF. The spatial distribution map of the DNN prediction did not show any obvious difference with that of the measured gravity. A good linear fitting of the SMV prediction to the measured gravity has been observed in tertiary only while that RF was good across all types of geology with best fitting in tertiary, then in cretaceous and, in quaternary. K-NN showed best linear fitting in the tertiary as for RF, followed by the quaternary instead of cretaceous. For DT, the linear fitting has been relatively good. In contrast to the other algorithms, DT prediction fits almost equally in all types of geology with a good tend in quaternary. In final, DNN showed the best of the best linear fitting across all types of geology. Its prediction fitted equally all types of geology in contrast to the other models with 0.996 Pearson correlation coefficient. The result of this study shows that machine-learning algorithms can be used to effectively, predict, and analyze gravity data in Kiri uplift region of the Congo sedimentary basin.

ACKNOWLEDGMENTS

The authors thank the department of geophysics of China University of petroleum (East China) for the support in terms of facilities and all anonymous readers for helping to improve the manuscript.

REFERENCES`

[1] W. Hinze, R. Von Frese and A. Saad, “The gravity method,” in *Gravity and Magnetic Exploration: Principles, Practices, and Applications*, Cambridge, Cambridge University Press, 2013, pp. 19-37.

[2] L. Thomas R. and N. Misac N., Fundamentals of gravity exploration, Tulsa: Society of Exploration Geophysicists, 2012.

[3] H. Lyatsky, “Gravity And Magnetic Geophysical Methods In Oil Exploration,” *Exploration & Production Magazine,* pp. 3-6, 10 March 2016.

[4] Z. Ming-hua, Q. Ji-hua, Z. Geng-xin and L. Xue-yi, “Regional gravity survey and application in oil and gas exploration in China,” *China Geology,* vol. 2, no. 3, pp. 382-390, 2019.

[5] K. Tondozi, M. J. Ntibahanana, M. Muyer, K. Bakamubia and M. Manzuma, “Spatial analysis of gravity anomalies in Cuvette Centrale sedimentary basin and contribution to the modeling of its petroleum system,” *International Journal of Innovation and Applied Studies,* vol. 21, no. 3, pp. 522-535, 2017.

[6] K. Tondozi, S. Maneno, S. K. Bahati, J. M. Ntibahanana and J. M. Ndombasi, “Interpretation of Magnetic Data for the Determination of Geological Structures in Southern Part of the Cuvette-Centrale Sedimentary Basin,” *International Journal of Advances in Scientific Research and Engineering,* vol. 6, no. 2, pp. 145-155, February 2020.

[7] S. Lawrence and M. Makazu, “Zaire's Central basin: prospectivity outlook,” *Oil Gas J.*, vol. 86, no. 38, pp. 105-108, 1888.

[8] M. Daly, S. Lawrence, D. Kimun'a and M. Binga, “Late Paleozoic deformation in central Africa: a result of distant collision,” *Nature*, pp. 605-607, 1991.

[9] P. Hoffman, “The breakup of Rodinia, birth of Gondwana, true poar wander and the snowball Earth,” *J. Afr. Eart Sci,* pp. 17-34, 1999.

[10] W. Kennedy, “The Structural Differentiation of Africa in the Pan-African (+/-500m.y.) tectonic episode.,” *Research Institute for African Geology, Leeds Univ. 8th Ann. Rep.*, pp. 48-49, 1964.

DOI: 10.31695/IJASRE.2022.8.7.3

[11] A. Kroner, A. Collins, E. Hegner, A. Willner, S. Muhongo and K. Kehelpannala, "The East African Orogen: New Zircon and Nd Ages and implications for Rodinia and Gondwana supercontinent formation and dispersal," *Gondwana Res.*, pp. 179-181, 2001.

[12] J. Visser and H. Praekelt, "Subduction, mega-shear systems and the late Paleozoic basin development in the African segment of Gondwana," *Geol. Rund.*, pp. 632-646, 1996.

[13] D. Delvaux, "Tectonic and palaeostress evolution of the Tanganyika-Rukwa-Malawi rif segment, East African Rift System," *Me.m.Mus. National Hist. Nat.*, pp. 545-567, 2001.

[14] A. Newton, R. Shone and P. Booth, "The Cape fold belt," *Geol. Soc. S. Africa*, pp. 521-530, 2006.

[15] F. Grant and G. West, Interpretation theory in applied geophysics, McGrawHill : Book Co., 1965.

[16] P. Vladimir, "Deep learning electromagnetic inversion with convolutional neural networks," *Geophysical Journal International*, vol. 218, p. 817–832, 2019.

[17] M. Everett and C. Weiss, "Geological noise in near-surface electronmagnetic induction data," *Geophys. Res. Lett.*, vol. 29, no. 1, pp. 101-104, 2002.

[18] B. Jason, Deep Learning with Python, Develop Deep Learning Models on Theano and TensorFlow using Keras, v1.18 ed., Melbourne: Machine Learning Mastery, 2019.

[19] W. Xinming, Y. Shi, F. Sergey, L. Luming and Uber, "Convolutional neural networks for fault interpretation in seismic images," in *SEG International Exposition and 88th Annual Meeting*, 2018.

[20] F. Wang, S. Chen and Y. Liu, "Deep learning for gravity and magnetic data interpolation," in *International Exposition and 89th Annual Meeting*, Texas, 2019.

[21] K. Noh, D. Yoon and J. Byun, "Imaging subsurface resistivity structure from airborne electromagnetic induction data using deep neural network," *Exploration Geophysics*, pp. 1834-7533, 2019.

[22] S. Maiti, R. K. Ch., P. Sarkar, T. R. K. and U. Srinu, "Interface depth modelling of gravity data and altitude variations: a Bayesian neural network approach," *Neural Computing and Applications*, vol. 32, p. 3183–3202, 2020.

[23] P. Dell'Aversana, B. Ciurlo and S. Colombo, "Integrated Geophysics and Machine Learning for Risk Mitigation in Exploration Geosciences," in *80th EAGE Conference & Exhibition 2018*, Copenhagen, Denmark, 2018.

[24] C. Laudon, "the 2019 Permian Basin Geophysical Society's 60th Annual Exploeration Meeting," *Geophysical Insights*, pp. 49-56, 2019.

[25] Nealon, E. Wang and Jeff, "Applying machine learning to 3D seismic image denoising and enhancement," *SEG*, pp. 131-139, 2019.

[26] P. Bas, H. Eldad and G. Justin, "Neural networks for geophysicists and their application to seismic data interpretation," *SEG*, pp. 534-540, 2019.

[27] Z. Wang, H. Di, M. A. Shafiq, Y. Alaudah and G. AlRegib, "Successful leveraging of image processing and machine learning in seismic structural interpretation: A review," *SEG*, pp. 451-461, 2018.

[28] A. Guitton, "3D convolutional neural networks for fault interpretation," 2018.

[29] X. Wu, S. Yunzhi, S. Fomel, L. Liang and Uber, "Convolutional neural networks for fault interpretation in seismic images," in *SEG International Exposition and 88th Annual Meeting*, 2018.

[30] Y. Shi, X. Wu and S. Fomel, "SaltSeg: Automatic 3D salt segmentation using a deep convolutional neural network," *SEG*, pp. 112-122, 2019.

[31] A. U. Waldeland, A. C. Jensen, L.-J. Gelius and A. H. S. Solberg, "Convolutional neural networks for automated seismic

DOI: 10.31695/IJASRE.2022.8.7.3

interpretation," *SEG*, pp. 529-536, 2018.

[32] L. Liu, L. Rong, L. Jianhai and W. Yang, "Seismic Lithofacies Computation Method Based on Deep Learning," *CGS/SEG International Geophysical Conference*, pp. 649-652, 2018.

[33] S. D. Mohaghegh, S. M. Al-Fattah and A. S. Popa, Artificial Intelligence and Data Mining Applications in the Exploration and Production Industry, USA: Society of Petroleum Engineers SPE, 2018.

[34] R. E. Neapolitan and X. Jiang, Artificial Intelligence With an Introduction to Machine Learning, 2nd ed., Boca Raton: Taylor & Francis Group, LLC, 2018.

[35] Z. Peng, L. Chengyan, L. Xiaolei, H. Weicong, W. Yulei and a. Z. Hualian, "Types of Diagenetic Facies of Tight Sandstone Reservoir and Its Quantitative Identification by Well Log Data," *The Open Petroleum Engineering Journal*, pp. p308-315, 2015.

[36] M. Venkatesan, "Artificial Intelligence vs. Machine Learning vs. Deep Learning," 7 May 2018. [Online]. Available: https://www.datasciencecentral.com/profiles/blogs/artificial-intelligence-vs-machine-learning-vs-deep-learning.

[37] J. Brownlee, 14 Different Types of Learning in Machine Learning, Melbourne, Australia: Machine Learning Mastery, 2019.

[38] S. Manohar, Mastering Machine Learning with Python in Six Steps: a practical implementation guide to predictive data analytics using python, Bangalore, Karnataka, India: Apress, 2017.

[39] I. Goodfellow, I. Bengio and A. Courville, "Deep Learning (Adaptative Computation and Machine Learning Serries)," *MIT Press*, 2016.

[40] C. M. Bishop, Pattern Recognition and Machine Learning (Information Science and Statistics), Germany: Spinger, 2006.

[41] S. Russell and P. Norvig, Artificial Intelligence: A Modern Approach, 3rd ed., Pearson, 2015.

[42] Alvishnu, "Generalisation and Overfitting," Machine Learning & AI Solutions in Hyderabad, 3 February 2017. [Online]. Available: https://wp.wwu.edu/machinelearning/2017/01/22/generalization-and-overfitting/. [Accessed 4 February 2021].

[43] P. Gupta, "Balancing Bias and Variance to Control Errors in Machine Learning," 5 May 2017. [Online]. Available: https://towardsdatascience.com/balancing-bias-and-variance-to-control-errors-in-machine-learning-16ced95724db. [Accessed 4 February 2021].

[44] M. Sharma, "Generalization in Machine Learning for better performance," 29 April 2019. [Online]. Available: https://mathanrajsharma.medium.com/generalization-in-machine-learning-for-better-performance-51bed74a3820. [Accessed 4 February 2021].

[45] L. Bottou and O. Bousquet, "The Tradeoff of Large Scale Learning," in *Optimization for Machine Learning*, Cambridge, MIT Press, 2012, pp. 351-368.

[46] L. Bottou, "Online Algorithms and Stochastic Approximations," *Online Learning and Neural Networks*, 1998.

[47] H. Geoffrey, "Divide the gradient by a running average of its recent magnitude," in *Lecture 6e rmsprop*, Canada, 2020.

[48] D. Kingma and J. L. Ba, "Adam: a Method for Stochastic Optimization," in *International Conference on Learning Representations*, 2015.

[49] M. Heusel, H. Ramsauer, T. Unterthiner, B. Nessler and S. Hochreiter, "GANs Trained by a Two Time-Scale Update Rule Converge to a Local Nash Equilibrium," *Advances in Neural Information Processing Systems 30 (NIPS)*, vol. 30, 2017.

[50] T. Dozat, "Incorporating Nesterov Momentum into Adam," *ICLR Workshop*, pp. 1-4, 2016.

[51] A. Mishra, "Metrics to Evaluate your Machine Learning Algorithm," Towards Data Science, 24 February 2018. [Online]. Available: https://towardsdatascience.com/metrics-to-evaluate-your-machine-learning-algorithm-f10ba6e38234. [Accessed 4 February 2021].

DOI: 10.31695/IJASRE.2022.8.7.3

[52] J. L. Mallet, "Numerical Earth Models," *European Association of Geoscientists and Engineers (EAGE Publications),* 2008.

[53] J. R. Fanchi, "Shared Earth Modelling: Methodologies for Integrated Reservoir Simulations," *Gulf Professional Publishing (Elsevier imprint),* pp. 10-306, 2002.

[54] N. Srivastava, G. Hinton, A. S. I. Krizhevsky and R. Salakhutdinov, "Dropout: a simple way to prevent neural networks from overfitting," *J. Mach. Learn. Res.,* vol. 15, no. 1, pp. 1929-1958, 2014.

[55] D. John, H. Elad and S. Yoram, "Adaptive Subgradient Methods for Online Learning and Stochastic Optimization," *JMLR,* vol. 12, pp. 2121-2159, 2011.

[56] L. Nettleton, Elementary gravity and magnetics for geologist and seismologists, Tulsa: Society of Exploration Geophysicists, 1971, pp. 24-46.

[57] D. Parasnis, Principles of applied geophysics, New York, USA: Chapman and Hall, 1986.

[58] E. Kadima, D. Delvaux, N. Sebagenzi, L. Tack and S. Kabeya, "Structure and geological history of the Congo basin: An integrated interpretation of gravity, magnetic and reflection seismic data," *Bassin Research,* vol. 23, pp. 499-527, 2011.

[59] A. Ohri, "8 Popular Regression Algorithms In Machine Learning Of 2021," 16 February 2017. [Online]. Available: https://www.jigsawacademy.com.

[60] J. Brownlee, Understand your data, create accurate models and work projects end-to-end., Melbourne, Australia: Machine Learning Mastery With Python, 2016.

[61] R. Sebastian and M. Vahid, Python Machine Learning, vol. 2, Birmingham: Packt Publishing Ltd, 2017.

[62] R. Rudolph, Step-by-Step Guide To Implement Machine Learning Algorithms with Python, 2018.

[63] D. Michie and D. Spiegelhalter, Machine Learning, Neural and Statistical Classification, C.C. Taylor, 1994.

[64] H. Lyatsky, "Magnetic and Gravity Methods in Mineral Exploration: the Value of Well-Rounded Geophysical Skills," *Geoscience Research & Consulting Ltd,* pp. 30-35, October 2010.

[65] E. Kadima, S. Sebagenzi and F. Lucazeau, "A Proterozoic-rift origin for the structure and the evolution of the cratonic Congo basin," *Earth and Planetary Science Letters,* pp. EPSL-10785; No of Pages 11, 2011.

[66] D. Amit, "The K-Fold Cross Validation in Machine Learning," 5 September 2020. [Online]. Available: https://www.knowledgehut.com.

[67] B. Jason, A Gentle Introduction to k-fold Cross-Validation, Melburne: Machine Learning Mastery, 2020.

[68] S. Sarath, "Pairplot vusualization," 29 September 2019. [Online]. Available: https://medium.com.

[69] Zach, "How to Calculate Correlation in Python," 3 July 2020. [Online]. Available: https://www.statology.org.

[70] D. A. Otchere, T. O. A. Ganat, R. Gholami and S. Ridha, "Application of supervised machine learning paradigms in the prediction of petroleum reservoir properties: Comparative analysis of ANN and SVM models," *Journal of Petroleum Science and Engineering,* p. 108182, 2020.

[71] D. Grana, L. Azevedo and M. Liu, "A comparison of deep machine learning and Monte Carlo methods for facies classification from seismic data," *Geophysics,* vol. 85, no. 4, pp. WA41-WA52, 2020.

[72] Y. Kim, R. Hardisty, E. Torres and J. Marfurt, "Seismic facies classification using random forest algorithm," in *SEG Technical Program Expanded Abstracts,* 2018.

[73] L. Zhang and C. Zhan, "Machine Learning in Rock Facies Classification: An Application of XGBoost," in *International Geophysical Conference,* Qingdao, 2017.

[74] Dell'Aversana, "Comparison of different Machine Learning algorithms for lithofacies classification from well logs,"

DOI: 10.31695/IJASRE.2022.8.7.3

Bollettino di Geofisica Teorica ed Applicata, vol. 60, no. 1, pp. 69-80, 2019.

[75] T. Zhao and P. Mukhopanpadhyay, "A fault-detection workflow using deep learning and image processing," in *88th Annual International Meeting*, Texas, 2018.

[76] A. Apoorva, "Loss Functions and Optimization Algorithms Demystified," 29 September 2017. [Online]. Available: https://medium.com. [Accessed 4 February 2021].

DOI: 10.31695/IJASRE.2022.8.7.3